Structure and dielectric properties of $Ba_2Cu_xY_{1-x}TaO_{6-y}$ double perovskite

F. S. Oliveira[1] · C. A. M. dos Santos[1] · A. J. S. Machado[1] · P. Banerjee[2] · A. Franco Jr.[3]

Abstract

In this paper, we reported the effect of Cu doping on the structural and dielectric properties of $Ba_2Y_{1-x}Cu_xTaO_{6-y}$ (0.00 $\leq x \leq$ 0.50) ceramics at room temperature. The copper for yttrium substitution reduces the sintering temperature and leads to structural changes in the Ba_2YTaO_6 rock-salt crystalline structure. Dielectric permittivity and complex impedance spectroscopy measurements suggested enhancement of the dielectric constant and occurrence of interfacial Maxwell–Wagner polarization.

Keywords Dielectric · Perovskite · Complex impedance spectroscopy

1 Introduction

Systematic analysis of $YBa_2Cu_3O_{7-\delta}$ (Y123) superconductor shows that Ta_2O_5 helps to achieve large-grains [1, 2] for the magnetic levitation and magnets applications [3–5]. The grain growth is attributed to the decrease in the peritectic temperature transformation [2], and the homogeneous segregation of Ba_2YTaO_6 (BYT) secondary phase in the Y123 superconducting matrix acts as vortex pinning centers, which are non-superconducting regions that confine the quantum magnetic flux, and consequently, optimizes the critical current density parameter [1, 6]. Furthermore, BYT phase also induces an unusual paramagnetic Meissner effect in Y123 superconductor [7].

Single crystals of BYT were grown by Galasso et al. using B_2O_3 flux in 1960s [8]. Later, the dielectric properties of BYT ceramic were studied in the microwave frequency range [9], and a structural phase transition [10] from cubic to tetragonal space group around 260 K was observed by diffractometry, calorimetry, transmission electronic microscopy, and Raman scattering [9, 11, 12]. This transition is quite similar to the $SrTiO_3$ antiferrodistortive case [13].

BYT belongs to the family of complex perovskite [14] oxides. This family group has attracted a lot of attention due to the presence of a large number of oxide materials which can be formed [15]. The long-range order of the crystal lattice is responsible for several properties in these complex perovskites [14, 15] such as the high dielectric permittivity [16, 17]. On the other hand, the extrinsic giant dielectric permittivity frequency observed in related perovskites such as $CaCu_3Ti_4O_{12}$ (CCTO) [18] is a consequence of semiconducting grains limited by insulating grain boundaries which act as a kind of barrier to the free carriers motion inside the grains [19–21]. The dielectric relaxation at these barriers of charge is well described by the Maxwell–Wagner (M–W) polarization model [22–24].

Since BYT appears as a secondary phase in Ta-doped Y123 [1], it suggests to one that Copper should have some solubility in the BYT complex perovskite, such as the $Ba_2Y_{1-x}Cu_xWO_{6-y}$ system already reported [25]. This paper presents the first investigation of the physical properties of $Ba_2Y_{1-x}Cu_xTaO_{6-y}$ system for 0.00 $\leq x \leq$ 0.50. Our results demonstrate that the sintering process, crystal structure, and dielectric relaxation change are

✉ F. S. Oliveira, fso@usp.br | [1]Escola de Engenharia de Lorena, Universidade de São Paulo, Lorena, Brazil. [2]Department of Physics, Gandhi Institute of Technology and Management (GITAM) University, Bengaluru, India. [3]Instituto de Física, Universidade Federal de Goiás, Goiânia, Brazil.

dependent of the sample composition. We also show that copper enhances the dielectric constant of BYT ceramics and leads to interfacial Maxwell–Wagner polarization at the grain boundaries. The extrinsic effects induced by Cu turn $Ba_2Y_{1-x}Cu_xTaO_{6-y}$ ceramics new candidates for some applications in electronic devices.

2 Experimental procedure

Ceramics of $Ba_2Y_{1-x}Cu_xTaO_{6-y}$ ($0.00 \leq x \leq 0.50$) were prepared by the standard solid state reaction method using $BaCO_3$ (Sigma-Aldrich, 99.95%) Y_2O_3 (Sigma-Aldrich, 99.99%) Ta_2O_5 (Cerac, 99.99%) and CuO (Sigma-Aldrich, 99.99%) powders. For each stoichiometry, powders were ball milled for about 12 h, then calcined at 950 °C in the air during 96 h. Approximately 10% in mass of polyvinyl alcohol (PVA) binder additive was added to the powders, and disk pellets with about 8 mm in diameter and 2 mm in thickness were pressed uniaxially. These pellets were annealed at 500 °C for 1 hour to decompose the organic PVA [26], and thereafter sintered in air at 1250 to 1400 °C for up to 120 h. The microstructure of ceramics was analyzed by scanning electron microscopy (SEM).

The crystalline structure of all samples was analyzed by XRD technique using Empyrean PANalytical diffractometer with CuKα radiation ($\lambda = 1.5406$ angstrons) and Ni filter. The diffractometry measurements were carried out with 0.01° step in $10° \leq 2\theta \leq 90°$ range. Model refinement profiles with Pseudo–Voigt function by Rietveld method were performed in HighScore Plus program using information from inorganic crystal structure database (ICSD) [27]. Both subdomain size and microstrain were obtained from Williamson–Hall plots [28–30]. The dielectric properties of the ceramic samples were studied using a computer controlled Agilent 4980A LCR meter. An alternating voltage of 1.0 V was applied on the ceramic pellets with silver painted faces over 20 Hz to 2 MHz frequency. Nyquist plots were analyzed using EIS Spectrum Analyzer program [31].

3 Results and discussion

The pure Ba_2YTaO_6 was formed only after long sintering time, 120 h at 1400 ° C, while the Cu-doped $Ba_2Y_{1-x}Cu_xTaO_{6-y}$ ($x = 0.40$) was formed after much shorter sintering time, 15 h at 1250 °C. Thus, it was evident that Cu for Y substitution lowers both sintering temperature and sintering time. Figure 1 shows that $x = 0.40$ sample (Fig. 1b) has signatures of liquid phase and more defects when compared with $x = 0.00$ sample (Fig. 1a). It is an evidence that the Cu concentration contributes significantly to the microstructure.
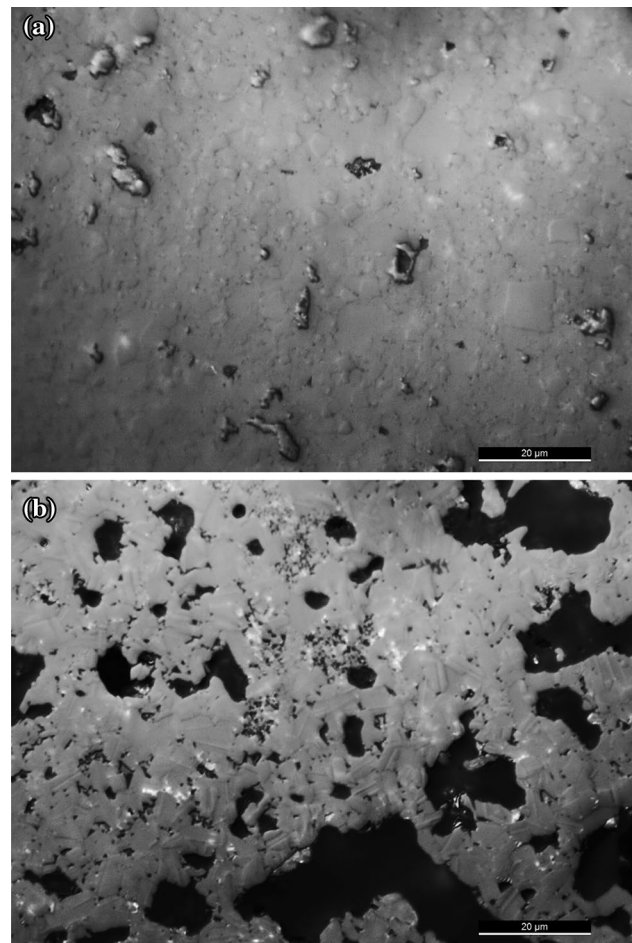

Fig. 1 SEM images for **a** $x = 0.00$ and **b** $x = 0.40$ sample

Figure 2 exhibits the XRD patterns for $x = 0.00$ and $x = 0.50$ samples. Our analysis suggests that the sample with the highest Cu doping level possesses a single cubic perovskite crystallographic phase. The lattice parameter of the undoped sample is in good agreement with those reported in literature [8, 9, 11, 12], and the decrease in the lattice parameter (see inset of Fig. 2b) can be attributed to the differences in the ionic radii of Cu^{2+} (0.73 angstrom) and Y^{3+} (0.9 angstrom) ions [32].

The Williamson–Hall plot shown in Fig. 3 gives the strain and the sub-cell domain information from the slope and the reciprocal of the intercept, respectively [28]. The Rietveld refinement results obtained for all samples are shown in Table 1. The Cu for Y substitution that produces compensating oxygen vacancies may induce strain in the crystal lattice. Additionally, XRD refinement also suggests that substitution increases the crystallite size in $Ba_2Y_{1-x}Cu_xTaO_{6-y}$ system.

In a double perovskite, the quantity of the long-range ordering degree (η) is given by [33]:
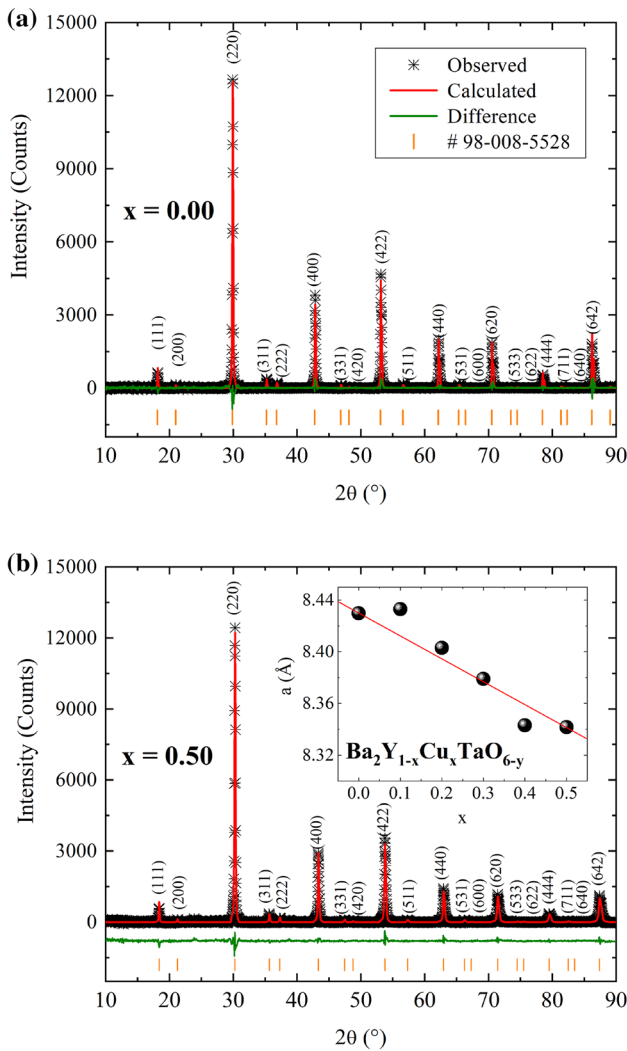
$$\eta = 2|M_0 - 0.5| \tag{1}$$

(a)

(b)

Fig. 2 **a** XRD pattern of $x = 0.00$ sample sintered at 1450 °C for 120 h. **b** XRD pattern of $x = 0.50$ sample sintered at 1250 °C for 15 h. The inset shows the Vegard's law dependence between lattice parameter and copper content
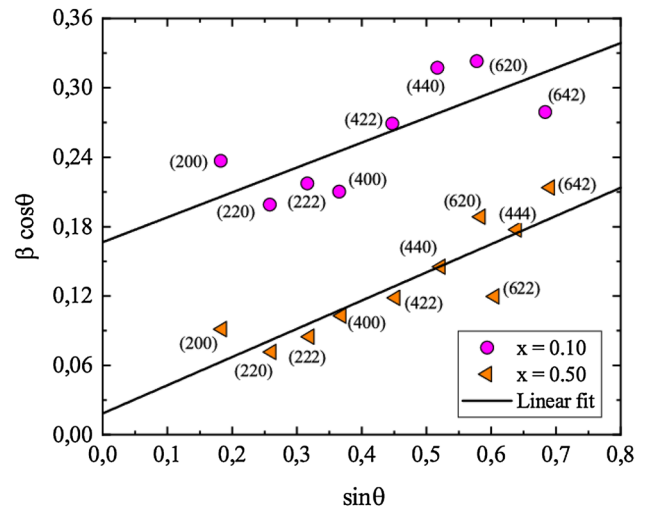

Fig. 3 Williamson–Hall plot of $x = 0.10$ and $x = 0.50$, where β is the full width at half maximum of the reflection peaks
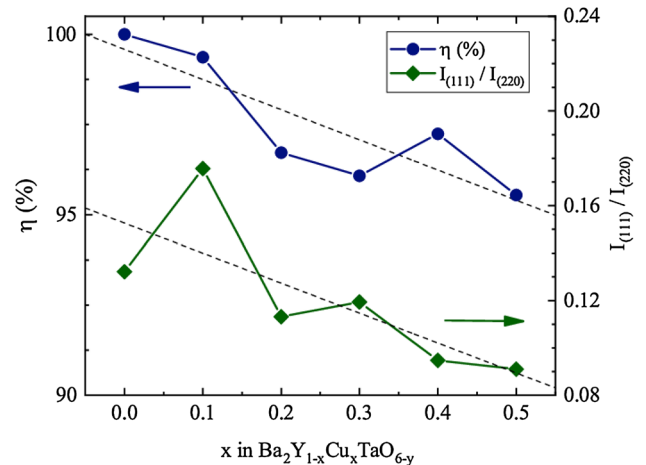

Fig. 4 Ordering degree (left-axis) and ratio between (111) and (220) peak intensities (right-axis). The dashed lines are just guides to the eyes

where M_0 is the refined occupation of Ta in the 4a (0,0,0) site or the refined occupation of Y or Cu in the 4b (1/2,1/2,1/2) site [28]. Beyond that, superlattice reflection peaks are sharper in high-ordered perovskites and the ordering degree is also related to the ratio between superlattice (odd,odd,odd) and sub-cell (even,even,even) peaks of the XRD pattern [33]. The results based upon both structure refinement and peak intensities of the XRD pattern suggest that the Cu for Y substitution may reduce the long-range ordering in BYT crystalline structure, as is shown in both Table 1 and Fig. 4.

The high dielectric permittivity observed in non-ordered double perovskites is understood in terms of randomic cation/valence long-range order distribution [14, 16]. In the $Ba_2Y_{1-x}Cu_xTaO_{6-y}$ system reported here, the ordering degree decreasing affects the distribution of both compensating oxygen vacancies and hole carriers within the grains [19]. It also offers considerable contributions for the dielectric relaxation [34–37].

Figure 5a shows the frequency dependence of real part of permittivity (ϵ') for $Ba_2Y_{1-x}Cu_xTaO_{6-y}$. It is evident that the low-frequency dielectric permittivity value for $x = 0.40$ ceramics at room temperature is higher than for $x = 0.00$. The initial high value of the real part of the dielectric permittivity could be due to the drop of applied voltage across the thin grain boundary widths, and space charge polarization is generated in $x = 0.40$ and $x = 0.50$ samples, which enhances the dielectric constant at the lower-frequency region.

Table 1 Rietveld refinement results as function as x in $Ba_2Y_{1-x}Cu_xTaO_{6-y}$. Refinement agreement factors: R_{exp} (expected) R_p (profile), R_{wp} (pondered profile), and goodness of fit (χ^2). Lattice parameter (**a**), crystallite size (D), strain (ϵ), ordering degree (η), and the ratio between (111) and (220) peak intensities

$Ba_2Y_{1-x}Cu_xTaO_{6-y}$						
x	0.00	0.10	0.20	0.30	0.40	0.50
R_{exp} (%)	5.11	5.69	5.13	6.48	4.62	5.13
R_p (%)	8.58	9.01	9.45	6.13	4.31	7.3
R_{wp} (%)	17.55	15.96	18.36	7.42	5.63	14
χ^2	3.42	2.81	3.58	1.14	1.22	2.73
a (Å)	8.423(1)	8.433(1)	8.403(1)	8.379(1)	8.343(1)	8.342(3)
D (Å)	973(229)	830(96)	1041(236)	1031(201)	4338(2590)	4795(2723)
ϵ (%)	0.05(4)	0.09(4)	0.04(2)	0.04(2)	0.09(3)	0.11(2)
η (%)	99.9	99.4	96.7	96.1	97.2	95.5
$I_{(111)} : I_{(220)}$	0.132	0.176	0.113	0.119	0.095	0.090

The initial high value of dielectric constant in Cu-doped samples indicates the presence of dc conductivity due to Maxwell–Wagner (M–W) relaxation process [23], which can be better visualized in the imaginary part (ϵ'') of the dielectric permittivity, as is shown in Fig. 5b. In accordance with Maxwell–Wagner (M–W) model, the imaginary part of dielectric permittivity can be written with the following expression [24],

$$\epsilon'' = \frac{1}{\omega C_0 (R_1 + R_2)} + \Delta\epsilon' \frac{\omega\tau}{1 + \omega^2\tau^2}, \quad (2)$$

where $\sigma = 1/C_0(R_1 + R_2)$ term is known as Ohmic conductivity (σ), where C_0 is a geometric factor, and R_1 and R_2 are the resistances of the real and imaginary dielectric components, respectively [23, 24]. The magnitude of the Ohmic conductivity can be determined from the slope of ϵ'' versus $1/\omega$ graph, as is shown in Fig. 5b inset where one can see that $x = 0.40$ has the higher conductivity. Equation 2 fits well with the experimental data which indicate the presence of M–W polarization. Hence, the oxygen vacancies generated due to the doping with Cu replacing Y increased the Ohmic conductivity for $x = 0.40$ and $x = 0.50$ samples as they diffused into the grain boundary regions, which enhances their dielectric constants at lower frequencies.

To understand the contribution of the interfacial polarization, complex impedance spectroscopy (CIS) was performed at room temperature. The phase angle of samples is shown in Fig. 6a.

In general, the approach of phase angle toward 90° represents the ideal poling state [38]. So it can be observed that slight addition of Cu enhances the poling condition $\sim 87°$ in the $x = 0.10$ ceramic samples. But the magnitude of phase angle for $x = 0.40$ was found to be $\sim 76°$. It suggests that sufficient amount of Cu in the Y site of Ba_2YTaO_6 crystalline structure leads to changes in poling state and domain switching.

The dependence of the impedance with frequency is shown in Fig. 6b on a double logarithmic scale. It can be observed that the magnitude of Z' decreases gradually for $x = 0.10$, $x = 0.20$, and $x = 0.30$ ceramics with the increase of ac frequency [39]. But for $x = 0.00$, $x = 0.40$, and $x = 0.50$ ceramics, the magnitude of $|Z|$ decreases gradually after 10 kHz frequency. The decrease of the real part of impedance at higher frequency domain and thereafter gradual merger suggests a possible release of space charge [40] from the ceramics.

Figure 7a shows the Nyquist plots for $Ba_2Y_{1-x}Cu_xTaO_{6-y}$ ceramics. Since the observed semicircles are non-centered, non-Debye type relaxation, i.e., Maxwell–Wagner relaxation, exists in these ceramics due to M–W relaxation [41].

An equivalent circuit shown in Fig. 7b may be represented by a bulk resistance (R_b) in series with a grain boundary resistance (R_{gb}), grain boundary capacitance (C_{gb}), and a constant phase element impedance (Z_{CPE}) in parallel as:

$$Z(\omega) = R_b + \left[\frac{1}{R_{gb}} + \frac{1}{\frac{1}{C_{gb}(j\omega)}} + \frac{1}{\frac{1}{P(j\omega)^n}} \right]^{-1} \quad (3)$$

In, $Z_{CPE} = 1/P(j\omega)^n$, P is the CPE parameter and n is the CPE element which behaves like a double-layer capacitor. The CPE is identical to a capacitance when $n = 1$ and to a simple resistance when $n = 0$ [42]. The experimental data fitted well with Eq. 3, establishing the validity of the equivalent circuit model. The single semicircle for each type of composition indicates the single conductivity mechanism in the ceramics. Table 2 shows the values of the fitting parameters for the ceramics samples.

It can be observed from the magnitude of Table 2 that for all samples, the CPE behaves like a parallel

Table 2 Electrical parameters of the equivalent electrical circuit obtained from complex impedance spectrum fits using Eq. 3 for $BaY_{1-x}Cu_xTaO_{6-y}$ samples

x	R_b (kΩ)	R_{gb} (MΩ)	C_{gb} (pF)	P (nFs^{n-1})	n
0.00	4.06	2.82	3.157	2.81	0.484
0.10	263.5	92.21	3.18	0.378	0.587
0.20	63.5	58.76	2.743	0.363	0.571
0.30	71.76	10.22	6.01	0.12	0.642
0.40	4.74	0.47	9.672	12.2	0.435
0.50	12.85	3.75	7.22	2.264	0.491

(a)

(a)

(b)

(b)

Fig. 6 **a** Dependence of phase angle with frequency at room temperature and **b** dependence of real part of impedance (Z′) with frequency at room temperature
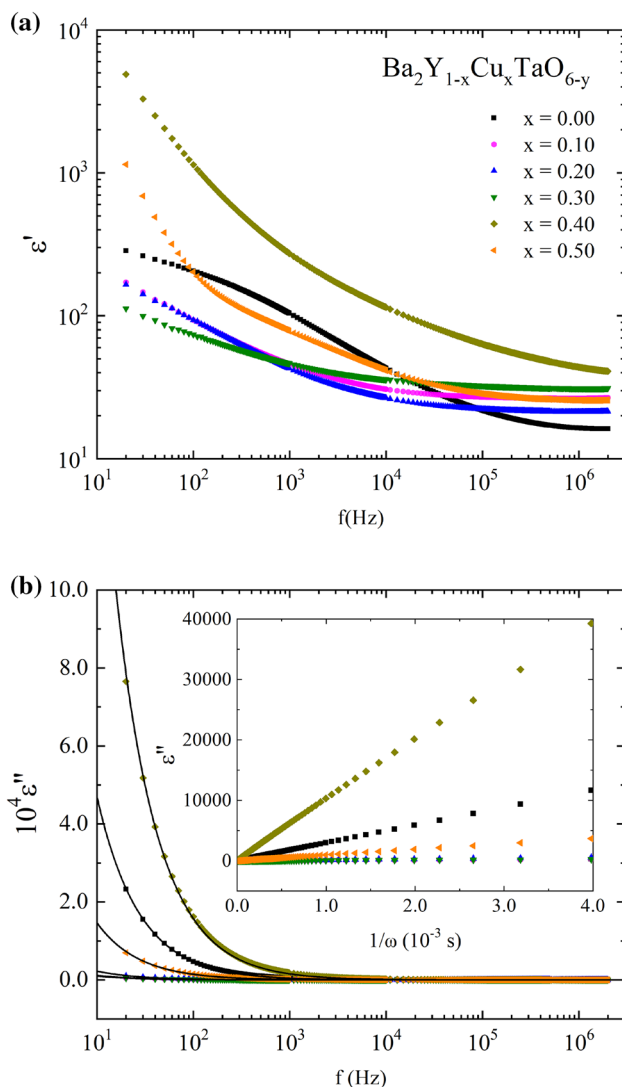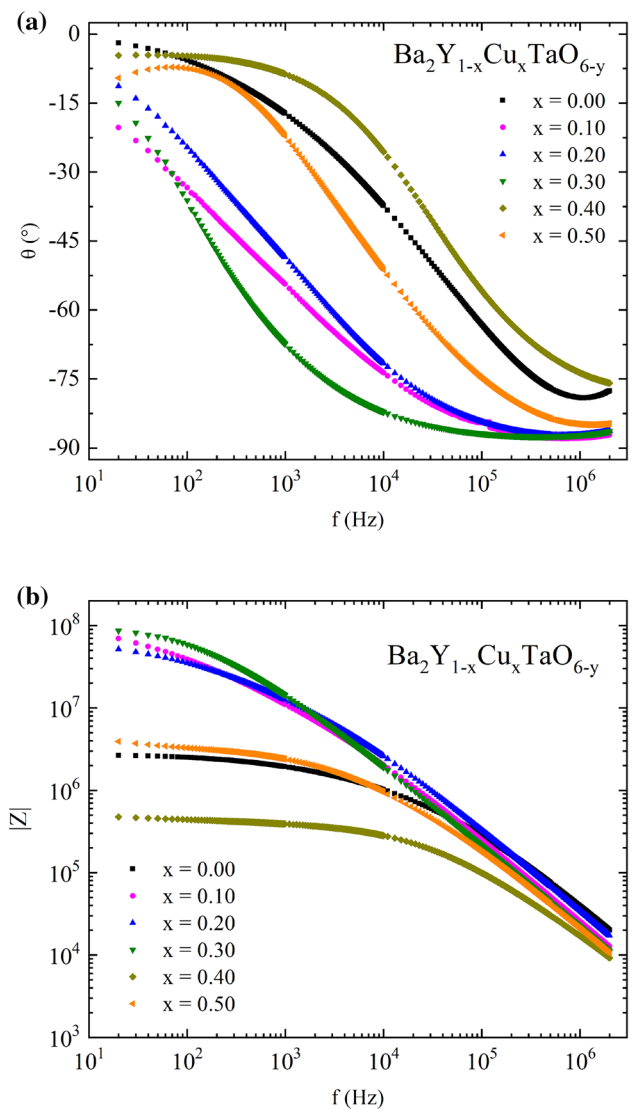
Fig. 5 Variation of **a** Real (ϵ') and **b** Imaginary (ϵ'') parts of permittivity with the variation of frequency at room temperature, the solid lines show the fitting with Maxwell–Wagner model using Eq. 2 and the inset shows ϵ'' as function as $1/\omega$

capacitor–resistor in the equivalent circuit [35]. With the addition of Cu in $Ba_2Y_{1-x}Cu_xTaO_{6-y}$, both resistance and capacitance of grain boundaries increase gradually which contribute to the barrier to the motion of charge carriers within large domain bulks of electrical resistance orders of magnitude lower than the boundaries resistance. Then, we conclude that it builds up a space charge polarization across the boundary regions which were represented by M–W model.
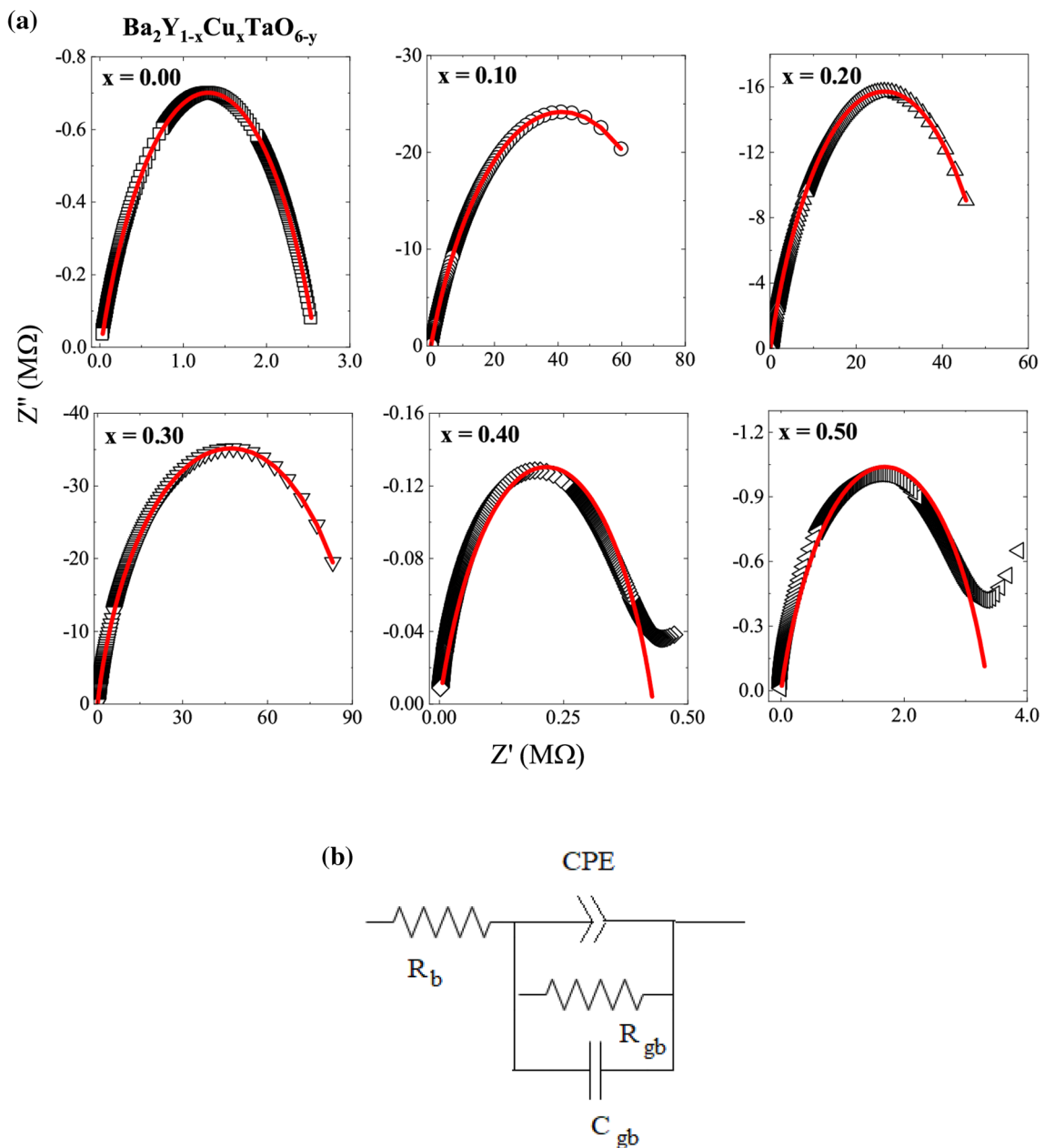
(a)

(b)

Fig. 7 **a** Nyquist plots for $Ba_2Y_{1-x}Cu_xTaO_{6-y}$ ceramics with $0.00 \leq x \leq 0.50$ (markers) and solid lines are fits using Equation 3. **b** Equivalent circuit used for fitting

4 Conclusions

Ceramics samples of $Ba_2Y_{1-x}Cu_xTaO_{6-y}$ with $0.00 \leq x \leq 0.50$ were studied by X-ray diffractometry, electronic scanning microscopy, dielectric permittivity measurements, and complex impedance spectroscopy. SEM images show liquid phase and defects induced by copper. The Rietveld refinement of the XRD patterns reveals systematic changes in the crystalline structure, ordering degree, and domain sizes with the Cu content. The complex dielectric permittivity measurement demonstrated that the dielectric relaxation of $Ba_2Y_{1-x}Cu_xTaO_{6-y}$ ceramics is described by the Maxwell–Wagner model. The complex impedance spectroscopy suggests that sufficient Cu for Y substitution in Ba_2YTaO_6 ceramics leads to changes in poling state and domain switching. The study also confirmed that the x value ($0.00 \leq x \leq 0.50$) in $Ba_2Y_{1-x}Cu_xTaO_{6-y}$ ceramics affected resistance and capacitance of grain boundaries which contributed to the barrier in motion of charge and build up a space charge polarization across the boundary regions.

Compliance with ethical standards

Conflict of interest The authors declare that they have no conflict of interest.

References

1. Oliveira CJV, Bortolozo AD, Ferreira B, dos Santos CAM, Machado AJS (2005) Effect of Ta_2O_5 addition on the texture of the y123 superconductor. Physica C 422(3–4):83–87

2. Bortolozo AD, Ferreira B, dos Santos CAM, Neves MA, Machado AJS (2004) Influence of the ta doping on the peritectic transformation of ybacuo superconductor. Physica C 408:876–878

3. Bondarenko SI, Koverya VP, Krevsun AV, Link SI (2017) High-temperature superconductors of the family $(Re)Ba_2Cu_3O_{7-\delta}$ and their application. Low Temp Phys 43(10):1125–1151

4. Siems SO, Canders WR, Walter H, Bock J (2004) Superconducting magnetic bearings for a 2mw/10kwh class energy storage flywheel system. Supercond Sci Technol 17(5):S229

5. Yu R, Mora J, Vilalta N, Sandiumenge F, Gomis V, Piñol S, Obradors X (1997) Effect of melt-processing temperature on the microstructure and the levitation force of ybco melt-textured superconductors. Supercond Sci Technol 10(8):583

6. Coll M, Guzman R, Garcés P, Gazquez J, Rouco V, Palau A, Ye S, Magen C, Suo H, Castro H, Puig T, Obradors X (2014) Size-controlled spontaneously segregated Ba_2YTaO_6 nanoparticles in $YBa_2Cu_3O_7$ nanocomposites obtained by chemical solution deposition. Supercond Sci Technol 27(4):044008

7. Dias FT, Vieira VN, Silva DL, Albino Aguiar J, Valadão DRB, Obradors X, Puig T, Wolff-Fabris F, Kampert E (2014) Paramagnetic moments in $YBa_2Cu_3O_7$ nanocomposite films. Physica C (Amsterdam, Neth) 503:175–177

8. Galasso FS, Layden GK, Flinchbaugh DE (1966) $Ba(B_{0.5}Ta_{0.5})O_3$ ordered perovskite-type compounds, possible new laser host materials. J Chem Phys 44(7):2703–2707

9. Zurmühlen R, Colla E, Dube DC, Petzelt J, Reaney I, Bell A, Setter N (1994) Structure of $Ba(Y_{1/2}^{+3}Ta_{1/2}^{+5})O_3$ and its dielectric properties in the range 10^2-10^{14} hz, 20–600 k. J Appl Phys 76(10):5864–5873

10. Karandeep HC, Gupta HC, Kumar S (2013) First principles study of structural and vibrational properties of Ba_2YTaO_6 in cubic and tetragonal phases. J Alloy Compd 555:335–338

11. Lufaso Michael W, Macquart René B, Lee Y, Vogt T, Loye H (2006) Pressure induced octahedral tilting distortion in Ba_2YTaO_6. Chem Comm 2:168–170

12. Zhou Q, Kennedy BJ, Kimpton JA (2011) The effect of disorder in Ba_2YTaO_6 on the tetragonal to cubic phase transition. J Solid State Chem 184(4):729–734

13. de Lima BS, da Luz MS, Oliveira FS, Alves LMS, dos Santos CAM, Jomard F, Sidis Y, Bourges P, Harms S, Grams CP, Hemberger J, Lin X, Faqué B, Behnia K (2015) Interplay between antiferrodistortive, ferroelectric, and superconducting instabilities in $Sr_{1-x}Ca_xTiO_{3-\delta}$. Phys Rev B 91(4):045108

14. King G, Woodward PM (2010) Cation ordering in perovskites. J Mater Chem 20(28):5785–5796

15. Vasala S, Karppinen M (2015) A2B B O6 perovskites: a review. Prog Solid State Chem 43(1–2):1–36

16. Yañez-Vilar S, Sánchez-Andújar M, Rivas J, Señarís-Rodríguez MA (2009) Influence of the cationic ordering in the dielectric properties of the La_2MnCoO_6 perovskite. J Alloy Compd 485(1–2):82–87

17. Chandrasekhar KD, Das AK, Mitra C, Venimadhav A (2012) The extrinsic origin of the magnetodielectric effect in the double perovskite La_2NiMnO_6. J Phys Condens Matter 24(49):495901

18. Subramanian MA, Li D, Duan N, Reisner BA, Sleight AW (2000) High dielectric constant in $CaCu_3Ti_4O_{12}$ and $CaCu_3Ti_3FeO_{12}$ phases. J Solid State Chem 151(2):323–325

19. Adams TB, Sinclair DC, West AR (2002) Giant barrier layer capacitance effects in $CaCu_3Ti_4O_{12}$ ceramics. Adv Mater 14(18):1321–1323

20. Tien TY, Cross LE (1967) Dielectric relaxation in strontium titanate solid solutions containing lanthania. Jpn J Appl Phys 6(4):459

21. Waser R (1991) Bulk conductivity and defect chemistry of acceptor-doped strontium titanate in the quenched state. J Am Ceram Soc 74(8):1934–1940

22. Wang G, Wang C, Huang S, Lei C, Sun X, Li T, Liu L (2013) Origin of colossal dielectric behavior in double perovskite Ba_2CoNbO_6. J Am Ceram Soc 96(7):2203–2210

23. Neill DO, Bowman RM, Gregg JM (2000) Dielectric enhancement and Maxwell–Wagner effects in ferroelectric superlattice structures. Appl Phys Lett 77(10):1520–1522

24. Banerjee P, Franco A Jr (2017) Substitution-induced near phase transition with Maxwell–Wagner polarization in $SrBi_2(Nb_{1-x}A_x)_2O_9$ ceramics [A = W, Mo, mo and x = 0, 0.025]. Physica Status Solidi (a) 214(10):1700067

25. Garcia-Ruiz A, Bokhimi, Portilla M (1992) Solid solutions in the $Ba_2Y_{1-x}Cu_xWO_{6-y}$ system. J Mater Res 7(1):24–28

26. Banerjee P, Franco A (2016) Rare earth and transition metal doped $BiFeO_3$ ceramics: Structural, magnetic and dielectric characterization. J Mater Sci Mater Electron 27(6):6053–6059

27. Belsky A, Hellenbrandt M, Karen VL, Luksch P (2002) New developments in the inorganic crystal structure database (icsd): accessibility in support of materials research and design. Acta Crystallogr B 58(3):364–369

28. Woodward P, Hoffmann RD, Sleight AW (1994) Order-disorder in $A_2M^{3+}M^{5+}O_6$ perovskites. J Mater Res 9(8):2118–2127

29. Alves TEP, Pessoni HVS, Franco A Jr (2017) The effect of Y^3+ substitution on the structural, optical band-gap, and magnetic properties of cobalt ferrite nanoparticles. Phys Chem Chem Phys 19(25):16395–16405

30. Dhahri A, Dhahri E, Hlil EK (2018) Electrical conductivity and dielectric behaviour of nanocrystalline $La_{0.6}Gd_{0.1}Sr_{0.3}Mn_{0.75}Si_{0.25}O_3$. RSC Adv 8(17):9103–9111

31. Bondarenko AS, Ragoisha GA (2005) Inverse problem in potentiodynamic electrochemical impedance. In: Pomerantsev AL (ed) Progress in chemometrics research. Nova Science Publishers, New York, pp 89–102 (the program is available online at http://www.abc.chemistry.bsu.by/vi/analyser/)

32. Shannon RD (1976) Revised effective ionic radii and systematic studies of interatomic distances in halides and chalcogenides. Acta Crystallogr Sect A Cryst Phys Diffr Theor Gen Crystallogr 32(5):751–767

33. Liu GY, Rao GH, Feng XM, Yang HF, Ouyang ZW, Liu WF, Liang JK (2003) Atomic ordering and magnetic properties of non-stoichiometric double-perovskite $Sr_2Fe_xMo_{2-x}O_6$. J Phys Condens Matter 15(12):2053

34. Yang WZ, Mao MM, Liu XQ, Chen XM (2010) Structure and dielectric relaxation of double-perovskite La_2CuTiO_6 ceramics. J Appl Phys 107(12):124102

35. Mahato DK, Sinha TP (2017) Dielectric, impedance and conduction behavior of double perovskite Pr_2CuTiO_6 ceramics. J Electron Mater 46(1):107–115

36. Rai HM, Saxena SK, Late R, Mishra V, Rajput P, Sagdeo A, Kumar R, Sagdeo PR (2016) Observation of large dielectric permittivity

and dielectric relaxation phenomenon in mn-doped lanthanum gallate. RSC Adv 6(32):26621–26629

37. de Sousa e Silva RL, Banerjee P, Junior AF (2019) Functional properties of donor-and acceptor-co-doped high dielectric constant zinc oxide ceramics. Phys Chem Chem Phys 21(18):9456–9464

38. Izquierdo JL, Bolanos G, Zapata VH, Moran O (2014) Dielectric relaxation and AC conduction in multiferroic $TbMnO_3$ ceramics: Impedance spectroscopy analysis. Curr Appl Phys 14(11):1492–1497

39. Kumari P, Rai R, Kholkin AL (2015) Influence of $BiFeTaO_3$ addition on the electrical properties of $Na_{0.4725}K_{0.4725}Li_{0.055}NbO_3$ ceramics system using impedance spectroscopy. J Alloy Compd 637:203–212

40. Sutar BC, Choudhary RNP, Das PR (2014) Dielectric and impedance spectroscopy of $Sr(Bi_{0.5}Nb_{0.5})O_3$ ceramics. Ceram Int 40(6):7791–7798

41. Barsukov Y, Macdonald JR (2012) Electrochemical impedance spectroscopy. Charact Mater 2:1–16

42. Shenglong Y, Bi H, Sun J, Zhu L, Huamin Y, Chunling L, Liu X (2019) Effect of grain size on the electrical properties of strontium and magnesium doped lanthanum gallate electrolytes. J Alloy Compd 777:244–251

Publisher's Note Springer Nature remains neutral with regard to jurisdictional claims in published maps and institutional affiliations.